JOURNAL OF AIRCRAFT
Vol. 44, No. 3, May–June 2007

Fatigue Testing of a Stiffened Lap Joint Curved Fuselage Structure

Abubaker Ahmed* and John G. Bakuckas Jr.†
Federal Aviation Administration William J. Hughes Technical Center, Atlantic City International Airport, New Jersey 08405
and
Jonathan Awerbuch,‡ Alan C. Lau,‡ and Tein-Min Tan‡
Drexel University, Philadelphia, Pennsylvania 19104

DOI: 10.2514/1.17162

In April 1988, Aloha Airlines flight 243 experienced an explosive midair decompression that resulted in the separation of an 18-foot section of the fuselage crown of the Boeing 737 airplane. Investigations revealed that the linkup of small cracks emanating from multiple rivet holes in a debonded lap joint contributed to the catastrophic failure. This cracking scenario, known as multiple-site damage, is one of two sources of widespread fatigue damage; a type of structural degradation characterized by the simultaneous presence of fatigue cracks at multiple structural elements that are of sufficient size and density whereby the structure will no longer meet its damage tolerance requirement. This study, sponsored by the National Aging Aircraft Research Program initiated by the Federal Aviation Administration in response to the Aloha accident, investigates multiple-site damage initiation and growth behavior in a pristine narrow-body fuselage panel. The test panel, a curved 6 × 10 ft stiffened structure containing six frames, seven stringers, and a longitudinal lap joint, was tested at the Federal Aviation Administration Full-Scale Aircraft Structural Test Evaluation and Research facility. The panel was subjected to a fatigue test with constant-amplitude cyclic loading, simulating the major modes of load associated with fuselage pressurization. Nondestructive inspections were conducted during the fatigue test to detect and monitor crack formation and growth. Multiple-site damage cracks were visually detected after about 80% of the fatigue life. Cracks developed and linked in the upper rivet row of the lap joint in the outer skin layer and formed a long fatigue crack before the termination of the fatigue test. A residual strength test was then conducted by subjecting the panel to quasi-static loads until catastrophic failure. Fractographic examinations were conducted to reconstruct crack growth history. Preliminary results show multiple crack origins and significant subsurface crack growth.

I. Introduction

MULTIPLE-SITE damage (MSD) is a source of widespread fatigue damage (WFD) that is characterized by the simultaneous presence of fatigue cracks in the same structural element [1]. Following the Aloha incident, considerable research efforts, sponsored by governments, industry, and academia worldwide, have focused on the causes and consequences of WFD and MSD. As a result, the presence of MSD in fuselage structures and its effects on the structural integrity are better understood. Yet, the detailed characteristics of the initiation and growth of MSD warrant further investigation.

Therefore, the primary focus of the current study is on MSD initiation, growth, and interaction in a full-scale pristine fuselage panel under simulated flight loading conditions. The test panel included a four-rivet-row longitudinal lap joint and a stiffening substructure consisting of six frames and seven stringers. The test was conducted at the Full-Scale Aircraft Structural Test Evaluation and Research (FASTER) facility at the Federal Aviation Administration (FAA) William J. Hughes Technical Center, Atlantic City International Airport, New Jersey. A quasi-static test was conducted before the fatigue test to ensure proper load introduction into the panel. The fatigue test was conducted by applying constant-amplitude loads that included programmed underload marker band cycles to enable the reconstruction of crack growth history from posttest fractographic analysis. MSD crack formation and growth were monitored and recorded using the self-nulling rotating eddy-current probe system and the remote-controlled crack monitoring (RCCM) system [2]. The fatigue test was terminated after observing rapid fatigue crack growth; the panel was then loaded quasi-statically up to final failure to determine its residual strength.

Fractographic examinations of the fracture surfaces in the panel were conducted to determine crack initiation sites and subsurface crack growth behavior. The fracture surfaces were examined under a scanning electron microscope (SEM) to map marker band locations. Crack lengths and crack growth rates were measured and compared with the visual measurements obtained from the RCCM system. The findings of the fractographic examinations correlated closely with visual observations of crack growth behavior recorded during the test.

II. Test Facility

As part of the National Aging Aircraft Research Program, the FASTER facility was established at the FAA William J. Hughes Technical Center for testing large curved panels representative of aircraft fuselage structure. The FASTER facility provides experimental data to validate and support analytical methods under development, including WFD prediction, repair analysis and design, and new aircraft design methodologies. The FASTER test fixture, Fig. 1, is capable of simulating flight loading conditions encountered by an aircraft fuselage by applying the major modes of loading,

Presented as Paper 2377 at the 46th AIAA/ASME/ASCE/AHS/ASC Structures, Structural Dynamics & Materials Conference, Austin, Texas, 18–21 April 2005; received 14 April 2005; revision received 27 March 2006; accepted for publication 15 May 2006.

*Federal Aviation Administration Drexel Fellowship Student; currently Boeing Commercial Airplane Group, Everett, WA 98203.
†Airworthiness Assurance Branch.
‡Department of Mechanical Engineering and Mechanics.

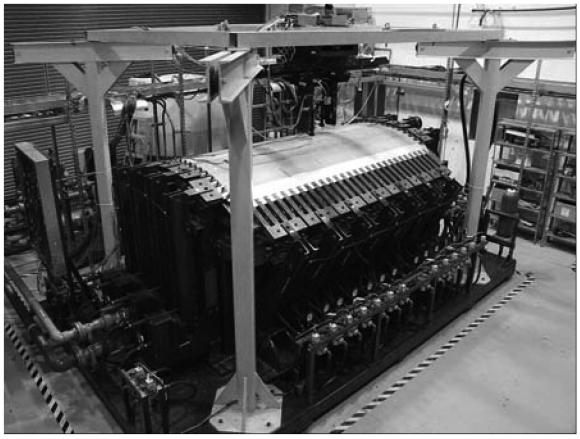

Fig. 1 Fuselage panel loaded on the FASTER test fixture.

including internal pressurization and the balancing tensile hoop, longitudinal, and frame loads. Both quasi-static and long-term durability spectrum loadings can be applied. The FASTER test fixture provides reliable and repeatable data in a cost-effective way. A detailed description of the FASTER facility and test fixture can be found in [2].

Two crack inspection methods, the self-nulling rotating eddy-current probe system and the RCCM system, were used to detect and monitor crack initiation and propagation. The rotating-probe system was developed to detect cracks hidden underneath countersunk rivet heads without having to remove the fasteners [3]. The system has a 15 MV output threshold; inspection signals exceeding the threshold indicate crack presence. Validation tests conducted at Sandia National Laboratories Aging Aircraft Nondestructive Inspection Validation Center showed that the rotating-probe system has a 90% probability of detection for a 0.032 in., first layer hidden crack [3]. The RCCM system is a video data acquisition system consisting of two computer-controlled, high-precision $x-y-z$ translation stages, each instrumented with a wide field-of-view camera and a narrow field-of-view camera. The combination of the two cameras allows the entire panel surface to be monitored at several levels of magnification, providing a field of view ranging from 0.05 up to 14 in. The translation stages of the RCCM system have a motion resolution of 0.00039 in. (1 μm), allowing accurate tracking of crack growth [2].

III. Panel Configuration

The full-scale curved panel tested in this study was representative of a narrow-body fuselage structure, Fig. 2. The dimensions of the panel were 120×68 in. with a radius of curvature of 66 in. The stiffening substructure of the panel included six frames extending in the circumferential direction with a 19 in. spacing and seven stringers in the longitudinal direction with a 7.5 in. spacing. The thickness of the 2024-T3 aluminum skin was 0.063 in. A longitudinal lap joint with two skin layers and two finger doubler layers was located in the middle of the panel along stringer S4. The lap joint contained four rivet rows, labeled A, B, C, and D, respectively, as shown in Fig. 2. Rivets were installed manually. Rivet types and pitch for each rivet row are shown in Table 1.

Table 1 Rivet types and pitch

	Rows A & D	Row B	Row C
Rivet type	MS20470AD5	MS20470AD6	NAS1097AD6
Rivet pitch, in.	1.5	0.813	0.813

The four edges of the panel were reinforced with aluminum doublers; holes were placed along the doublers so that the hoop and longitudinal load assemblies could be attached to the panel. The two ends of each frame, where the frame load assemblies are attached, were also reinforced with aluminum doublers. An elastomeric seal was bonded along the perimeter of the inner surface of the curved panel to attach to the pressure box of the FASTER fixture. The panel was instrumented with 64 strain gauges to monitor and record strain distribution during the test. Strain gauges were installed on the skin, frames, and stringers. Several back-to-back strain gauge sets were installed at various locations on the skin to measure local bending.

IV. Test Procedure

A. Applied Loads

The test was conducted in three phases using the loading conditions shown in Table 2. Loads representative of an elevated cabin pressurization condition were applied to the panel, including internal pressure and the balancing tensile loads in the hoop and longitudinal directions. A maximum internal pressure of 16 psi was applied in phases 1 and 2 of the test resulting in a hoop load of 1056 lb/in. and a longitudinal load of 528 lb/in. in the panel. The hoop load was divided between the skin and the frames by a ratio of 83.2:16.8, which was determined from finite element analyses [4]. The resulting maximum net hoop stress in the skin was about 14.0 ksi. A companion test program, sponsored by the FAA and the U.S. Air Force (USAF), investigated crack initiation and progression in flat 2024-T3 aluminum panels with similar lap joint configurations subjected to a cyclic tensile load of 15.0 ksi [5]. The selection of the applied loads in the current study enables direct comparison of the strain distribution and fatigue crack growth behavior with the results of the companion flat panel study.

In phase 1, loads were applied quasi-statically using either air or water as the pressurization medium. Strains were measured and recorded and the strain distribution was studied to ensure proper load

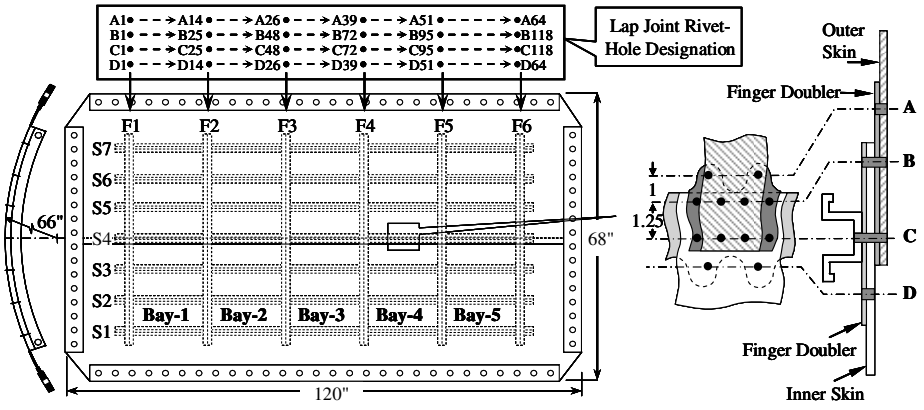

Fig. 2 Panel dimensions and lap joint configuration.

Table 2 Test phases and applied loads

Test phase	Purpose	Load type	Maximum loads			
			Pressure, psi	Hoop, lb/in.	Frame, lb/in.	Long., lb/in.
1	strain survey	quasi-static	16.0	878.6	177.4	528.0
2	fatigue crack growth	cyclic, $R = 0.1$[a]	16.0	878.6	177.4	528.0
3	residual strength	quasi-static	loads incremented up to catastrophic failure			

[a]$R =$ the stress ratio (the ratio of the minimum to the maximum applied pressure).

transfer from the fixture to the test panel and to identify locations in the panel where cracks were likely to initiate.

In phase 2, an accelerated fatigue test, at a loading frequency of about 0.04 Hz, was conducted. For safety reasons, water was used as the pressurization medium. A constant-amplitude load spectrum was applied to the panel, including underload cycles, to generate marker bands on the fracture surfaces so that crack growth history and crack front shapes could be reconstructed from posttest fractographic examinations. The load spectrum, shown in Fig. 3, consisted of three baseline blocks of 1000 cycles at an internal pressure of 16.0 psi. Each of the baseline blocks was followed by a group of marker cycles including either 6, 4, or 10 iterations of 100 underload cycles at 12.0 psi pressure, separated by spikes of 10 16 psi cycles. Each group of marker cycles generates a corresponding number of marker bands on the fracture surface, thus enabling correlation between subsurface crack sizes and the number of load cycles. The load spectrum was applied throughout the fatigue test. The 6–4–10 marker band spectrum was applied in the companion FAA/USAF flat panel study and was found effective in marking 2024-T3 aluminum fracture surfaces without adversely affecting crack growth behavior. Crack history reconstruction of crack sizes as small as 0.0008 in. has been reported. However, due to fracture surface damage during fatigue loading or final fracture (e.g., fretting between the two crack surfaces), the smallest crack size measured ranged on average from 0.004 to 0.02 in. [5].

In phase 3 of the test, the residual strength of the damaged panel was determined by applying loads quasi-statically until final failure. The internal pressure applied to the panel was increased in 2 psi increments up to 14 psi and in 1 psi increments thereafter. Strain gauge measurements and crack lengths were recorded continuously throughout the residual strength test.

B. Fractographic Examinations

Fractographic examinations of the crack surfaces in the test panel were conducted to reconstruct crack growth histories. After the test was completed, the panel was removed from the test fixture and specimens prepared for crack surfaces examinations under the SEM. Because of the final cracking configuration of the panel, crack surfaces in the upper rivet row of the lap joint were readily removable without having to break the rivets. A rough global cut was made using a cutting wheel to remove four bays of the free skin on the upper side of the crack. A band saw was then used to make precision cuts to remove individual specimens. A detailed cleaning procedure was followed: first, the rivet hole specimens were soaked in acetone and then in a water-based acidic surface cleaner. To prevent chemical etching of the fracture surfaces, the specimens were then immersed in a water-based alkaline cleaner. As a final step, the specimens were cleaned in acetone and then thoroughly rinsed in distilled water. All cleaning was done in an ultrasonic cleaner to avoid inadvertently damaging the fracture surfaces.

The fracture surfaces were examined using an FEI/Phillips XL30 SEM with a field-emission electron gun. The procedure for mapping the locations of marker bands on the fracture surface was as follows: a local Cartesian x–y coordinate system was established on the fracture surface with the origin (0, 0) chosen at a reference point that could be readily identified under the SEM. Points along each marker band were then recorded relative to the origin. For each marker band, sufficient points were recorded to characterize its location and local curvature directions. All recorded points were then plotted in two-dimensional space; crack sizes and crack growth rates were measured directly from the marker band plots. A similar procedure was employed by Willard [6].

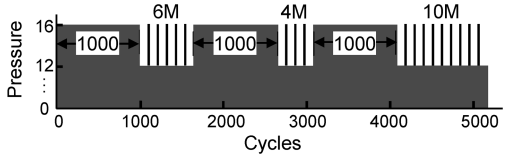

Fig. 3 Marker band spectrum used in the fatigue test.

V. Results and Discussion

A. Phase 1, Strain Survey

Strain distributions in the panel were recorded under the quasi-static loading conditions described in Table 2. Strain gauge measurements compared very well with the results of a full-scale verification test conducted on an aft fuselage section of a narrow-body aircraft, thus verifying proper load transfer into the panel from the FASTER test fixture [7].

Back-to-back strain gauge sets were installed at several locations on the skin to measure local bending. The schematic in Fig. 4 shows the locations of the four back-to-back gauge sets: at a skin midbay location (gauge set 33), at a distance of 0.5 in. above rivet row A (gauge set 38), midway between two rivets in row A (gauge set 39), and 0.5 in. below rivet row D (gauge set 45). Measurements of the membrane strain (the average of the strain measurements at the inner

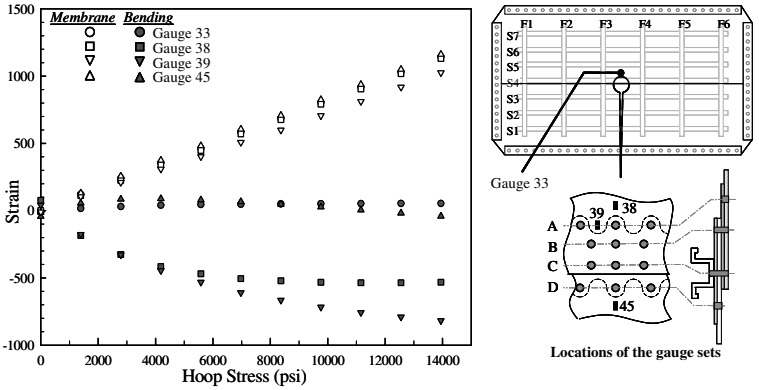

Fig. 4 Membrane and bending strain measured at four locations on the skin.

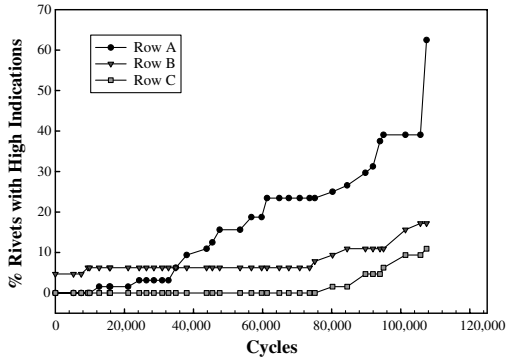

Fig. 5 Percentage of rivet holes in lap joint with crack indications using eddy current.

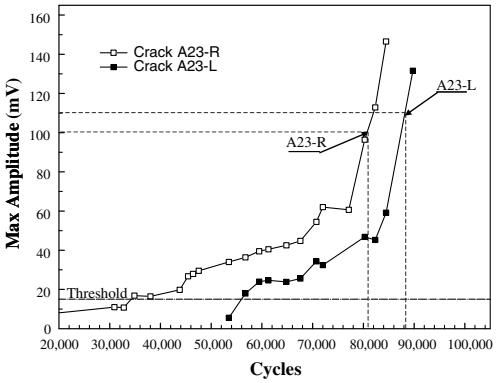

Fig. 7 Change in maximum amplitudes of eddy-current signals recorded at rivet holes A22 and A23.

and outer surfaces) and bending strain (half of the difference between the inner and outer surface measurements), at the four locations, are shown in Fig. 4. The membrane strain was nearly the same at all four locations. The bending strain differed significantly depending on the location. The highest bending strain was recorded by gauge set 39 along rivet row A. As a result of the local bending, the inner surface of the skin along rivet row A of the lap joint experienced high tensile stresses, making this rivet row a likely area for damage initiation.

B. Phase 2, Fatigue Test

During the fatigue test, crack formation in the lap joint was monitored and recorded using the rotating-probe eddy-current system and the RCCM system. Eddy-current indications of subsurface damage in rivet row A were recorded as early as 12,600 cycles (Fig. 5). As shown in the figure, the number of rivets in row A with high-level signals increased with fatigue cycles. A few high-level signals were also detected in rows B and C. Rivet row D was not accessible for reliable inspection with the rotating-probe system during the test because of the joint's geometry.

Damage was first visually detected via the RCCM system after 51,500 fatigue cycles. A crack was detected on the rivet head of rivet A23, located in the upper rivet row between frames F2 and F3 (Fig. 6a). Similar rivet head cracks were detected at seven other rivets in row A. Fractographic examinations of the rivet head crack showed marker bands and striations indicating fatigue failure due to cyclic pressure applied by the skin on the countersunk rivets in row A, where high local bending was measured [8].

After 80,550 cycles, a skin crack (designated A23-R) was visually detected on the right-hand side of the rivet hole A23 at a distance from the edge of the rivet hole (for clarity, open circles were inserted to indicate crack tips in the photographs of Fig. 6). Crack A23-R grew in both directions (Fig. 6b) and eventually linked up with the rivet hole (Fig. 6c). At a later stage, a second skin crack (designated A23-L) was visually detected on the left-hand side of rivet hole A23

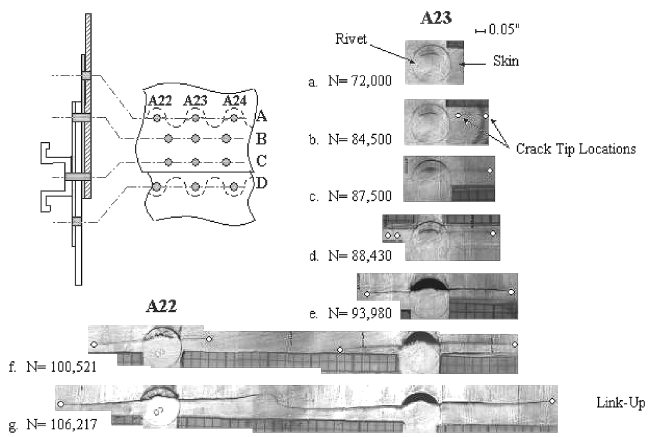

Fig. 6 Crack growth process in outer critical rivet row.

(Fig. 6d), also at a distance from the rivet hole. Crack A23-L also grew in both directions and linked up with the rivet hole (Fig. 6e). Cracks developed in a very similar way at the neighboring rivet, A22 (Fig. 6f). At 106,217 fatigue cycles, cracks from rivet holes A22 and A23 linked up and formed a 2.87 in. crack (Fig. 6g).

All four cracks emanating from rivet holes A22 and A23 were detected by high eddy-current signals before they were visually detected. The plot in Fig. 7 summarizes the results of eddy-current inspections of rivet hole A23. High-level signals were first detected on the right-hand side of A23 after 35,000 cycles, well before crack A23-R was visually detected at 80,550 cycles. At 55,000 cycles, eddy-current inspections indicated the presence of damage on the left-hand side of A23, where crack A23-L was visually detected at 88,390 cycles. The increase in the amplitude of the inspection signals is an indication of subsurface crack growth. Eddy-current inspection results were correlated with the subsurface crack growth history reconstructed by fractographic examinations (as discussed next).

Crack growth after the first linkup of MSD between rivets A22 and A23 at 106,217 cycles (crack length = 2.87 in.) is shown schematically in Fig. 8. Shortly after the first linkup, cracks were detected emanating from rivet hole A24. Cracks A24-L and A24-R were detected at 106,644 and 106,680 cycles, respectively (Figs. 8b and 8c). Unlike the cracks at A22 and A23, the two cracks at rivet hole A24 were completely linked to the rivet hole when first observed. Additionally, due to crack interaction and stress redistribution, cracks A24-L and A24-R grew relatively faster than the cracks detected earlier at rivet holes A22 and A23. The second crack linkup occurred at 106,930 cycles when the lead crack (formed between A23 and A22) and crack A24-L grew past each other and formed a football-shaped ligament before linkup (Fig. 8d). After 109 additional fatigue cycles (at 107,039 cycles), the lead crack grew into rivet hole A21 to the left (Fig. 8e). No cracks were visually observed at rivet hole A21 before the linkup. Subsequently, there was a notable increase in the crack growth rate of the lead crack at both ends (Figs. 8f–8j). At 107,425 fatigue cycles, the lead crack extended to the right through rivet hole A26 and linked up to one of the existing cracks at shear-clip rivet hole F3-5 (observed earlier at 79,915 cycles) (Fig. 8k). As a result of linkup to the cracks at F3-5, the lead crack crossed over into the third skin bay and became a two-bay crack. Soon thereafter, a short crack (crack A27-L) was observed on the left-hand side of rivet hole A27 (Fig. 8l). At that time, the lead crack also grew into rivet hole A19 to the left. It took only eight additional fatigue cycles (at 107,445 cycles) for the lead crack to link up with crack A27-L and reappear on the right side of rivet hole A27. Simultaneously, the left crack tip propagated through rivet hole A18 (Fig. 8m). At 107,458 fatigue cycles, the lead crack was spanning across rivet holes A17 to A27 with a total length of 16.04 in. (Fig. 8n). Considerable crack growth was observed during each of the final few fatigue cycles. Therefore, the fatigue test was terminated at 107,458 cycles for postfatigue residual strength test [8].

Figure 9 shows the length of the lead crack (measured visually via the RCCM system) as a function of the number of fatigue cycles. Crack length measurements were recorded relative to a reference line

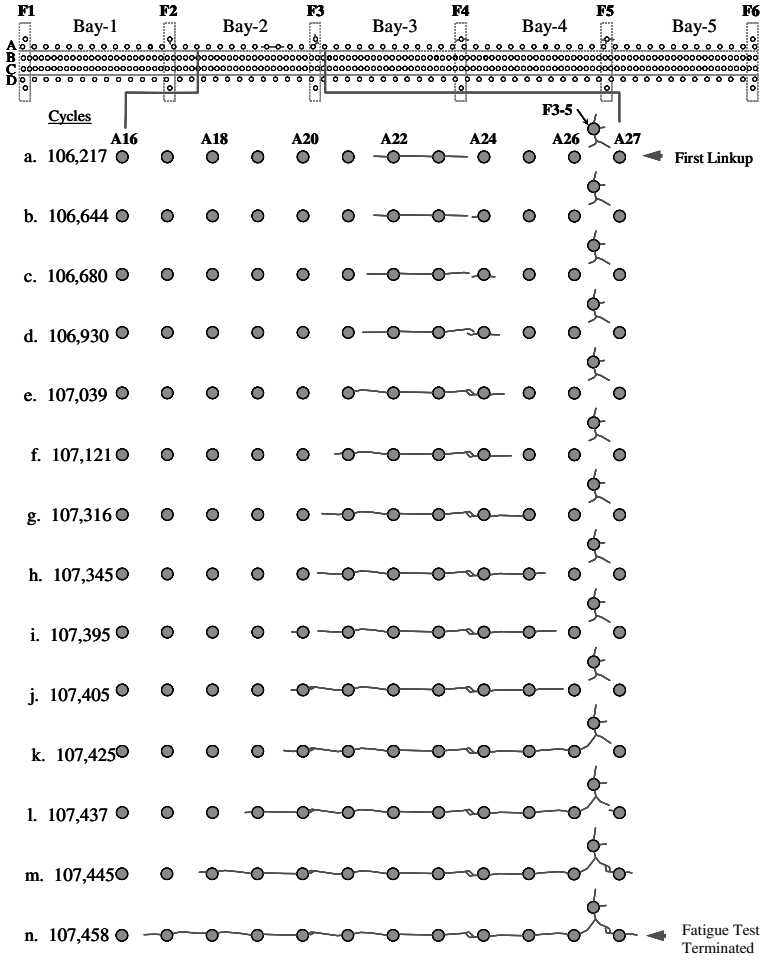

Fig. 8 Crack progression along rivet row A following the first linkup.

midway between rivet holes A22 and A23 where the first crack linkup occurred. It can be seen that the lead crack initially grew at approximately the same rate to the left and to the right of the reference line. On the right-hand side, as the crack tip approached frame F3, the growth rate decreased, as expected. However, the growth rate of the left-hand side of the crack, which was propagating toward the midbay, continuously increased. The lead crack extended along the upper rivet row of the lap joint mainly in the second bay and crossed over frame F3 slightly into the third bay to a final length of 16.04 in.

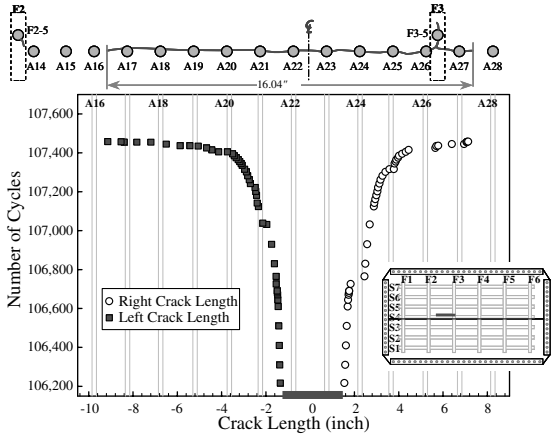

Fig. 9 Growth of the right and left crack tips of the lead crack during the fatigue test.

C. Phase 3, Residual Strength Test

After terminating the fatigue test, the panel was subjected to quasi-static pressurization up to failure to determine its residual strength. Loads were applied quasi-statically with a pressure increment of 2 psi up to 14 psi and an increment of 1 psi thereafter. Further crack extension was observed at 16 psi pressure, which was the maximum applied pressure during the fatigue test. Catastrophic failure of the joint occurred at a pressure of 17.8 psi. The lead crack abruptly extended to a five-bay, 75 in. long crack. Figure 10 shows the final state of damage after the residual strength test. To the left, the lead crack extended to frame F2, linked up with the crack at shear-clip rivet hole F2-5, and stopped about 0.5 in. past that shear-clip rivet hole. To the right, the crack extended much further and was arrested between rivets A62 and A63 close to frame F6.

As the crack propagated primarily along rivet row A, the panel exhibited very limited crack-turning or flapping capabilities. At the locations of frames F4 and F5, the crack turned upward and linked up with the cracks emanating from shear-clip rivet holes F4-5 and F5-5 before turning downward to continue extending along rivet row A. A posttest inspection on the inner surface of the panel showed that frames F3, F4, and F5 were completely fractured under the lap joint. The damage at frame F4 is shown in Fig. 10. Further examinations of frame failures are currently underway.

D. Results of Fractographic Examinations

Fractographic examinations were conducted to determine crack initiation sites and subsurface crack growth behavior. Preliminary results are discussed here for crack A23-R which was visually detected on the right-hand side of rivet hole A23 at 80,550 fatigue cycles. The SEM images in Fig. 11 show a general view of the crack surface and a close-up view of the region near the rivet hole and along

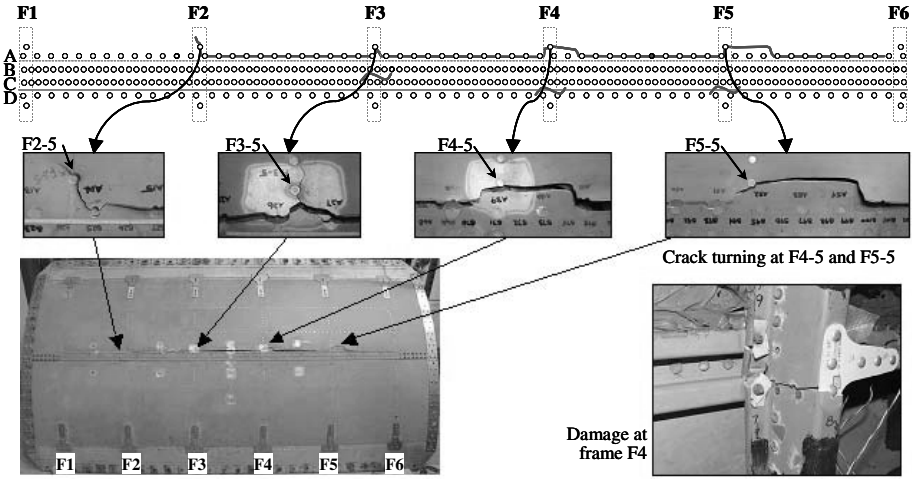

Fig. 10 Final state of damage at the end of the residual strength test.

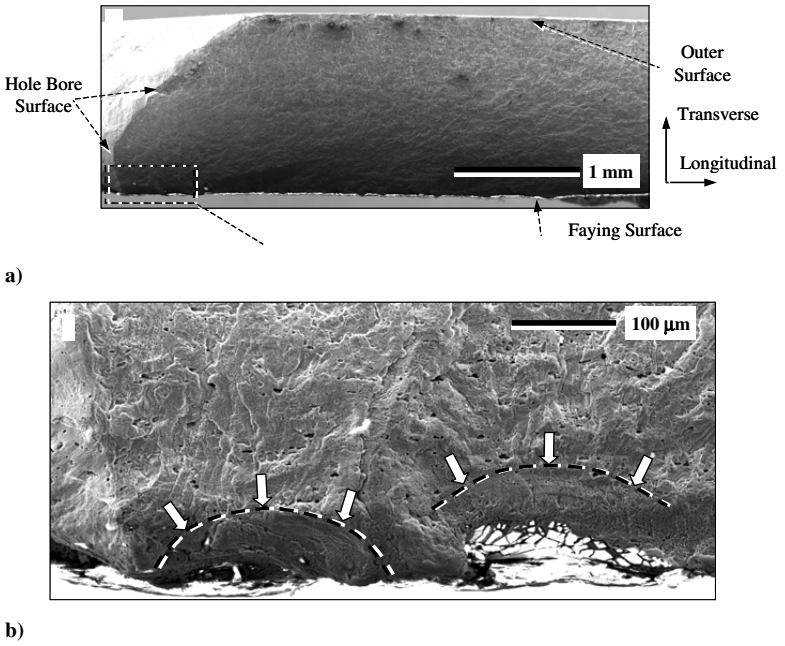

Fig. 11 SEM images of crack A23-R showing a) a wide view of the fracture surface, and b) a closeup of crack origin locations along the faying surface.

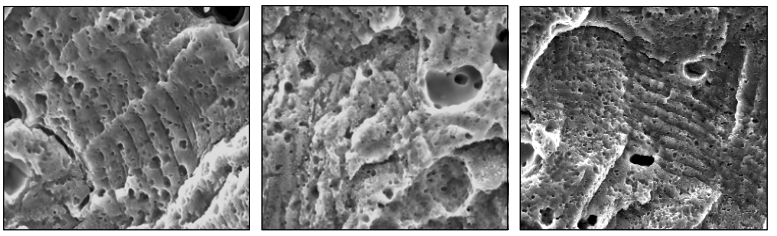

Fig. 12 SEM images of showing the appearance of marker band groups.

the faying surface (the inner surface of the outer skin mating with the finger doubler). Multiple crack origins were identified in the vicinity of the rivet hole indicating that the crack resulted from the coalescence of multiple small cracks. The locations of crack origins on the faying surface were characterized by the presence of surface damage that, apparently, occurred either during joint installation or as a result of fretting with the doubler during fatigue loading. Surface damage and the high tensile hoop strains resulting from secondary bending along rivet row A (Fig. 4) would contribute to crack initiation along the faying surface.

Marker bands, generated by applying the load spectrum shown in Fig. 3, were readily detectable under the SEM at magnification levels ranging from 350X to over 3500X, depending on the crack size. In general, the groups of 10-marker bands (10M) were easier to follow, whereas the groups of four-marker bands (4M) were somewhat more challenging. Examples of SEM images of all three marker band groups are shown in Fig. 12. Near the locations of crack origins, where multiple cracks grew independently, marker bands were more difficult to interpret. Further down the fracture surface, marker bands became easier to identify and trace nearly across the entire thickness

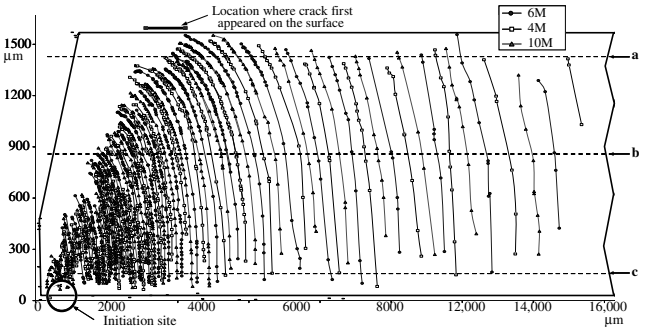

Fig. 13 Marker band locations for crack A23-R.

of the skin. Marker bands were detectable up to a faying-surface crack length of about 0.63 in. (16 mm) beyond which the fracture surface became dominated by large fatigue striations, indicating rapid crack growth.

To reconstruct subsurface crack growth history, the locations of marker bands for crack A23-R were plotted (Fig. 13). For clarity, a thickness-to-length ratio of about 2:1 has been used in the plot. The location where the crack was first visually detected on the outer surface of the skin is indicated in the figure. Crack front shapes were, in general, part-elliptical with the major axis lying along the faying surface and the minor axis in the thickness direction. Marker bands were tracked back to the location of crack origins at the faying surface near the corner of the rivet hole. In the region surrounding the countersink of the hole, where residual compressive stresses from the rivet clamp were dominant, no marker bands or fatigue striations were detected. The absence of marker bands and striations indicates that the area around the countersink of the rivet hole remained uncracked as the subsurface crack propagated to the outer surface of the skin. Eventually, when the tensile stress at the crack tip became sufficient to overcome the residual compressive stresses, the countersink area ruptured.

Subsurface crack lengths and crack growth rates were measured directly from the plot of marker bands. Measurements were made in the longitudinal direction at three different depths across the skin thickness, as indicated by the three horizontal dashed lines in Fig. 13: near the free surface (line a), along the geometric centerline of the skin (line b), and near the faying surface (line c). The number of load cycles associated with each marker band was determined by correlation with visual measurements recorded during the fatigue test [8].

Fractographic and visual crack length measurements for crack A23-R are plotted as a function of load cycles in Fig. 14. As seen, the fractographic measurements near the free surface (along line a in Fig. 13) correlated very well with the visual crack measurements, validating the fractography data reduction process. The fractographic results also indicated that crack A23-R existed as early as approximately 19,000 cycles. The subsurface crack length measured along the faying surface at that number of cycles was 0.015 in., which is within the range of 0.004–0.02 in. of the smallest crack length

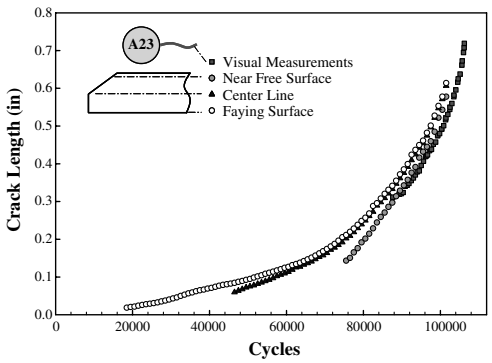

Fig. 14 Crack lengths from fractographic examinations and visual measurements.

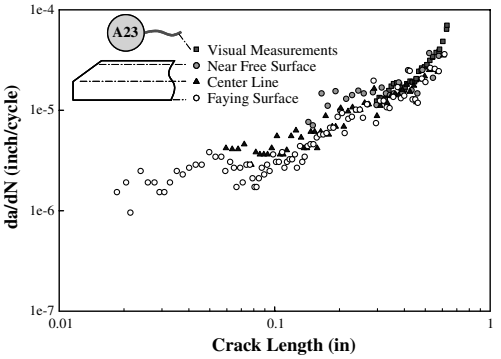

Fig. 15 Crack growth rates from fractographic examinations and visual measurements.

reconstructed in [5] for flat aluminum panels with similar joint configurations.

Using the rotating eddy-current probe system, crack A23-R was first detected at 35,000 cycles (Fig. 7). From the marker band reconstruction of the crack history, the crack length, measured near the faying surface, was approximately 0.05 in. after 35,000 cycles (Fig. 14). As mentioned earlier, the rotating-probe system has a probability of detection of 90% for a 0.032 in. hidden crack. A complete correlation of the results of the rotating-probe inspections with the fractographic examination results is underway.

Crack growth rates da/dN as a function of crack length for crack A23-R are plotted in Fig. 15. The plot shows growth rates measured in the longitudinal direction near the faying surface, along the centerline, and near the free surface together with the visual measurements. As expected, crack growth rates increased with the crack length. Additionally, fractographic measurements correlated very well with the visual measurements of crack growth rates.

VI. Conclusions

The initiation, growth, and interaction of MSD in a pristine, curved fuselage panel containing a longitudinal lap joint were investigated. The test panel was subjected to a constant-amplitude fatigue loading using the Full-Scale Aircraft Structural Test Evaluation and Research facility located at the Federal Aviation Administration William J. Hughes Technical Center. Strain survey tests were conducted to ensure proper load introduction into the panel. During the fatigue test, damage formation and growth in the lap joint were monitored and recorded in real time using the rotating eddy-current probe system and high-magnification visual inspections. Cracks were initially detected in the upper critical rivet row of the lap joint by eddy-current inspections after 12,600 cycles. Visible cracks in the lap joint eventually developed in the outer skin sheet after 80,550 cycles. The first MSD linkup occurred after 106,217 cycles, resulting in a 2.87 in. lead crack. Subsequently, the lead crack grew very rapidly along the upper rivet row into a two-bay, 16.04-in.-long crack after 107,458 cycles, at which point the fatigue test was terminated. A residual strength test was conducted by applying quasi-static loads to determine the load-carrying capacity of the panel. Catastrophic failure occurred at a pressure of 17.8 psi when the lead crack extended instantaneously across five bays to a final length of 75 in. without much crack turning or flapping. Three frames were fractured under the lap joint.

Fractographic examinations were conducted for the first visually detected crack in the lap joint (crack A23-R) to determine initiation sites and to reconstruct subsurface crack growth behavior from marker band locations. The results from this single crack revealed multiple initiation sites and extensive damage along the faying surface of the skin. A map of the locations of marker bands showed that crack A23-R existed as early as 19,000 cycles. Because of extensive damage along the faying surface, high bending stresses, and residual compressive stresses around the rivet hole, crack A23-R grew substantially along the faying surface before becoming a visible, through-the-thickness crack. Crack lengths and crack growth rates, measured from fractography, correlated very well with the

visual measurements made during the test. Despite the complexity of the structure of the fuselage panel tested in the current study and the applied loading, fractographic examinations provided a clear and complete reconstruction of crack growth history. Additional fractographic examinations are being conducted for this as well as the remaining cracks in the lap joint.

Acknowledgments

The first and the last three authors would like to express their sincere appreciation to the Federal Aviation Administration William J. Hughes Technical Center for its support through the Federal Aviation Administration–Drexel Fellowship Research Grant (97-G-032) to Drexel University. The first author would also like to thank Ramesh Ramakrishnan of Delta Air Lines for his guidance during the initial phase of the fractographic study. In addition, thanks are due to Carlos Calderon and Socheth Bith of the Mechanical Engineering and Mechanics Department of Drexel University for their help with the fractographic examinations.

References

[1] McGuire, J., and Foucault, J., "Recommendations for Regulatory Action to Prevent Widespread Fatigue Damage in the Commercial Airplane Fleet," Final Rept. of the Airworthiness Assurance Working Group, 1999.

[2] Bakuckas, J. G., Jr., "Full-Scale Testing and Analysis of Fuselage Structure Containing Multiple Cracks," U.S. Dept. of Transportation/ Federal Aviation Administration AR-01/46, July 2002.

[3] Wincheski, B., Simpson, J., and Todhunter, R., "New Instrument for the Detection of Fatigue Cracks Under Airframe Rivets," *Review of Progress in Quantitative Nondestructive Evaluation*, Vol. 16, Pt. B, 1997, pp. 2113–2121.

[4] Anderson, B., Hsu, C., Carr, P., Lo, J., Yu, J., and Duong, C., "Evaluation and Verification of Advanced Methods to Assess Multiple-Site Damage of Aircraft Structure," U.S. Dept. of Transportation/ Federal Aviation Administration AR-04/42,I, Oct. 2004.

[5] Fawaz, S. A., "Equivalent Initial Flaw Size Testing and Analysis," U.S. Air Force Research Lab. VA-WP-TR-2000-3024, 2000.

[6] Willard, S. A., "Use of Marker Band for Determination of Fatigue Crack Growth Rates and Crack Front Shapes in Pre-Corroded Coupons," NASA CR-97-206291, 1997.

[7] Ahmed, A., Bakuckas, J. G., Jr., Bigelow, C. A., Tan, P., Awerbuch, J., Lau, A., and Tan, T., "Initiation and Distribution of Multiple-Site Damage in a Fuselage Lap Joint Curved Panel," *Proceedings of the 6th Aging Aircraft Conference, San Francisco, CA, 2002* [CD-ROM], Paper 2A1, 2002.

[8] Ahmed, A., and Bakuckas, J., "Development of Multiple-Site Damage in Fuselage Structure," U.S. Dept. of Transportation/Federal Aviation Administration AR-05/38, Sept. 2005.